Detection of Direct-path Arrivals for Multi-Narrowband Sequences (3-30 kHz) In Shallow Water

A. Zoksimovski, C. de Moustier

Center for Coastal and Ocean Mapping, University of New Hampshire
24 Colovos Road, Durham, NH 03824

Abstract. In an effort to measure underwater acoustic transmission loss over direct-path lengths ranging from a few hundred meters to ten kilometers in shallow water, a sequence of 16 gated pure tones (3-30 kHz) was transmitted every 10 s from a towed source and received at moored sonobuoys. The magnitude of multipath arrivals often exceeded that of direct-path arrivals, resulting in variable detection performance of simple matched filtering techniques. More reliable signal recognition was obtained via iterative least square time constraints on the arrival times across all frequencies in a sequence, based on the known time intervals between transmitted tones. Signal detection improvement was obtained also by searching for the direct-path arrival near the global maximum of the sum of the rectified correlograms of the received sequences. These methods allowed detection in environments characterized by multipath interferences, as well as low signal-to-noise ratio and fading, and in the presence of other unrelated sonar signals that cause large detection errors. It also improved the direct-path signal strength estimation, and associated transmission loss computation, by bounding the time interval over which to compute the signals' autocorrelations and estimate their power. These algorithms were tested on a limited data set recorded in the Southern California Offshore Range, confirming that frequencies below 6 kHz suffered less direct-path transmission losses than higher frequencies (7-30 kHz).

INTRODUCTION

Efficient underwater acoustic communication depends on the selection of a frequency band that is well adapted to the propagation channel. In shallow water environments, this channel is characterized by rapid changes, with range and depth, in the physical properties of the ocean volume and its boundaries. A measure of the frequency response of the channel can be obtained by estimating the transmission loss over a specified path at a range of frequencies. In the following, we shall focus on acoustic frequencies from 3 kHz to 30 kHz and report on direct-path transmission loss measurements over ranges extending to a few kilometers.

The experimental data were collected at three sites in the Southern California Offshore Range, West of San Clemente Island, in December 2000, and in February and June 2001. Two sites were in water depths ranging from 100 m to 300 m: one was between Cortes and Tanner Banks (32°41'N/119°11.07'W), and the other was South of San Clemente Island's China Point (32°45.17'N/118°25'W). The third site was in deep water (1600 m) in San Nicholas Basin (32°55'N/118°54'W). The environmental

part of the experiment included conductivity/temperature/depth measurements, as well as shipboard and moored acoustic Doppler current profiles.

The acoustic signals were transmitted from an omni-directional transducer (ITC-1007) [1] towed by a ship, and were recorded at two identical SSQ-57B sonobuoy hydrophones [2] deployed on a mooring line at 27.4 m and 61 m depths. The intent was to place one hydrophone in, and one below the mixed layer, which is the upper nearly uniform portion of the sound speed vs. depth profile. Likewise, the source was towed in and below the mixed layer. In the Southern California Bight, the depth of the mixed layer decreases from about 50 m in January, to around 20 m in April [3]. During the experiment, the base of the mixed layer was typically found between 10 m and 40 m below the sea surface. However, the mixed layer was not always strongly defined and the depth of its base varied along the transmission path.

A transmission sequence consisted of 16 continuous wave (CW) pulses at discrete frequencies ranging from 3 kHz to 12 kHz in 1 kHz steps, and from 12 kHz to 30 kHz in 3 kHz steps. Each tone lasted 10 ms, with a 90 ms gap between pulses. The complete sequence lasted 1.6 s, followed by a 10 s quiescent period before the next transmission sequence, yielding a repetition period of 11.6 s for single frequency tones.

As shown in Fig. 1, the transmitter source level ranged from 173 to 195dB re 1 µPa @ 1 m when driven at constant power. The transmitted signals were recorded also at an omni-directional reference hydrophone (ITC-1042) [1], attached on the towing line 3 m away from the source in order to monitor the source levels. To avoid saturation of the highly sensitive sonobuoy receivers (Fig. 1) when approaching them, source levels were reduced in 10 dB steps from the maximum values shown in Fig. 1.

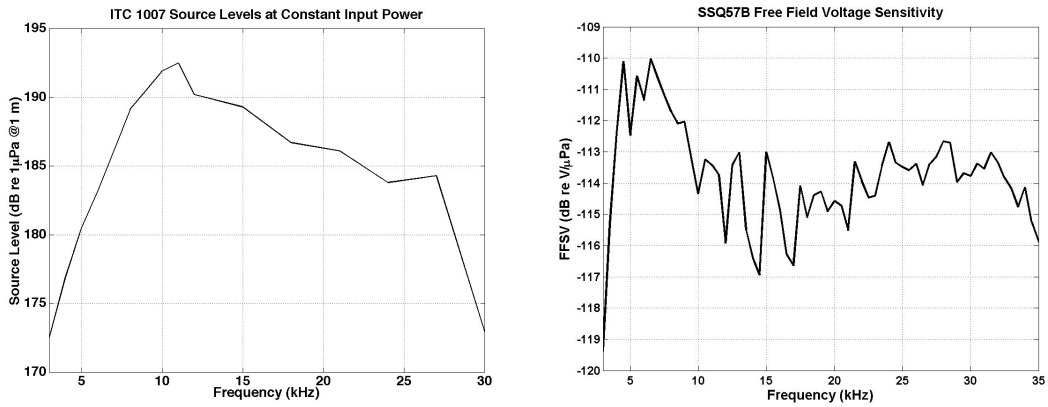

(a) (b)

FIGURE 1. Source Level calibration of the ITC-1007 transducer (a) and Free Field Voltage Sensitivity calibration of the SSQ-57B receiver (b).

The ship towed the source at about 2.5 m/s on orthogonal traverses roughly 18 km long, and centered on the hydrophones mooring. At each ping, the direct-path transmission loss, TL, across the distance that separated the reference hydrophone and the two moored hydrophones was estimated by taking the ratio of their respective received sound intensities I_0 and $I_{1,2}$, according to [4, Chapter 5]:

$$TL = 10\log_{10}\left(\frac{I_0}{I_{1,2}}\right) \quad dB \tag{1}$$

To first order, underwater acoustic transmission loss includes spreading and absorption losses. In shallow water, spreading losses at range R can be spherical ($20\log_{10}R$) or cylindrical ($10\log_{10}R$), whereas absorption losses vary with local temperature and increase in proportion to the square of the acoustic frequency [4]. Other factors of acoustic field attenuation are refraction, reflections from the seafloor and the sea surface, the various kinds of sound channels existing in the sea, and the multipath effects causing fluctuations in sound reception.

In this experiment, direct arrival detection could not be achieved with conventional detection algorithms, such as matched filter or maximum likelihood methods [5-7], because of the high correlation between the multipath and direct-path signals, and because the multipath arrivals often were stronger than the direct-path arrivals. To overcome this problem, we have devised two different detection methods based on combined frequency analysis. One method relies on a least square time constraint applied to all 16 signals in a sequence. The other uses the sum of the rectified auto-correlograms of the transmitted pulses as a detection template to search for the direct-path arrival near the global maximum of the sum of the rectified correlograms of the received time series. We describe the characteristics of the received time series in Section II, and present the algorithms for our direct-path arrival detection methods in Section III. Examples of the resulting estimates of transmission loss versus range and frequency are given in Section IV.

SIGNAL PROPERTIES

A typical spectrogram of the received signal is shown in Fig. 2. The received signals stand out in intensity at the corresponding frequencies. Acoustic intensity exceeding 120 dB re 1 μPa was detected at each transmitted frequency with longer duration than the transmission time of each pulse (10 ms). The extended time of each received signal is mostly the result of reflections from the seafloor and sea surface. Because of the limitations of the acoustic source used (Fig. 1), the transmitted power was stronger at the mid frequencies (8-12 kHz) than at the others, with a maximum at 11 kHz. Therefore, it takes longer for the acoustic field to settle back to the ambient noise level after the transmission period for pulses near 11 kHz. Higher harmonics of some frequencies, e.g. 7, 8, 9, 10 kHz, due to clipping of the multipath signals, are observable as well in Fig. 2. Most notably, the strong third harmonics of these frequencies (21, 24, 27, and 30 kHz) fall in transmission bands and can cause detection errors at those frequencies.

Interference from signal replicas that arrive at the receiver as reflections from objects or surfaces, e.g. schools of fish, water surface or bottom, presents another critical obstacle for smooth processing of the received signal. In shallow water, this phenomenon is not as uniformly distributed in range as noise, but is range and location dependent due to relatively close boundaries. Fig. 3 shows a sequence of consecutive

pulses at the same frequency, for both moored hydrophones. Assuming an average speed of the ship around 2.5 m/s, 6 pings yield a travel path of 6×1.6×2.5 = 174 m.

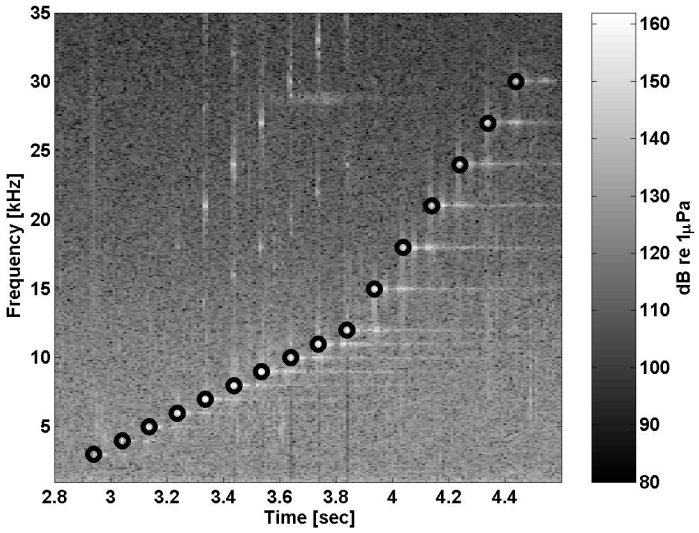

FIGURE 2. Spectrogram of the time series received at one hydrophone for one transmission sequence (range ≅ 2 km). Circles identify direct-path arrivals, and trailing signals represent multipath arrivals.

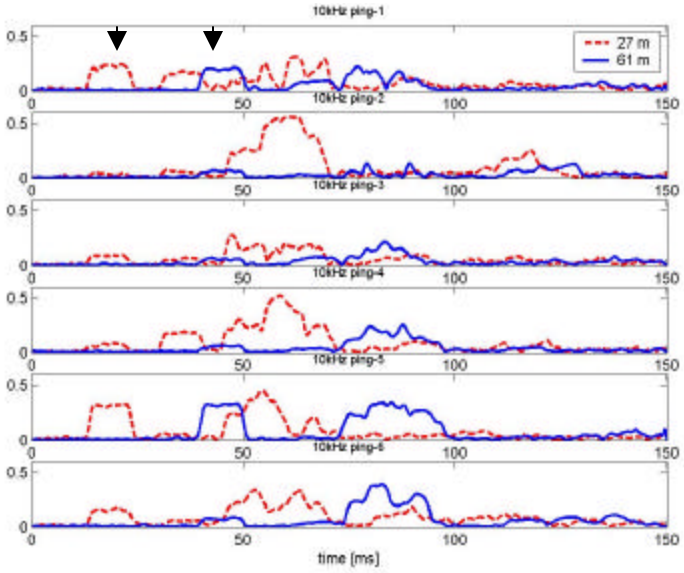

FIGURE 3. Pressure envelope (units of Pa) of 6 consecutive pings from measurements made at the Cortes-Tanner Banks site. Depths for the source and the receiving hydrophones were respectively about 40 m, 27 m, and 61 m. The arrows point to the first arrivals of the signals at the two different receiver depths.

We can see that within a 174 m difference in range, the direct-path pressure magnitude fluctuates between 0 and 0.5 Pa. In addition, the multipaths have different patterns at 61 m and 27 m, thus interferences vary with depth. Nonetheless, the magnitude of the direct-path signal is very similar at the two depths. This should not

be the case if the source and the shallower of the receivers were inside the mixed layer, because the wave front would be mostly trapped inside the layer [4].

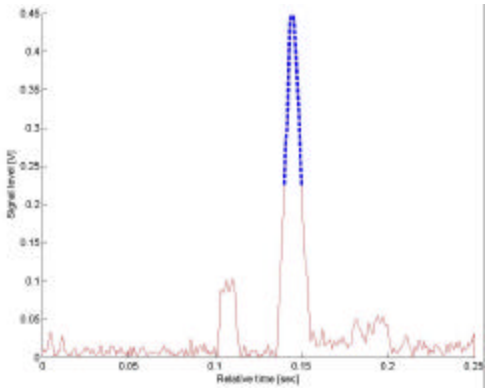

FIGURE 4. Envelope of a received signal with a strong multipath component. The direct-path arrival starts at 0.1 s and the taller peak starting at 0.13 s is due to multipath. The dashed line is the envelope of the signal detected by matched filtering.

SIGNAL DETECTION METHODS

In Fig. 4, the direct-path signal is followed by a few reflections. Because of the additional loss at the boundaries, the reflected acoustic waves are expected to have lower magnitude than the original [8]. Besides dynamic change in shape and magnitude from location to location (Fig. 3), this type of undesired signal, called acoustic echo [5] or multipath [6][7], is highly correlated to the direct-path signal. If a matched filter [5] were applied to this kind of pattern, it would almost definitely recognize the reflection with maximum magnitude as the most probable direct-path signal, which is incorrect in this example. In order to overcome this problem, we have devised and implemented two different algorithms: one based on a least square time constraint applied to the arrival times in a sequence, and the other based on the sum of the rectified correlograms of the received signals.

Least Square Time Constraint

Observing that multipath is a relatively random phenomenon (Fig. 3), a regular pattern would not be expected in the time difference between the direct-path arrival and reflections at N different frequencies. Therefore, we devised a method that detects each CW pulse independently, and then applies a tone-to-tone time constraint to get a more accurate estimate of the direct-path arrival times of the pulses, and to help distinguish direct arrivals from reflections. The algorithm contains the following steps applied to each received transmission sequence:

1) Band-pass filtering, centered at each of the transmitted frequencies. The bandwidth of each band-pass filter should be at least as wide as the associated Doppler shift Df (Hz), which for a ship speed v_s = 2.5 m/s, sound speed c = 1500 m/s, and acoustic frequency f_m (Hz), is given by:

$$\Delta f = v_s f_m / c \approx f_m / 600 \ \ (Hz) \tag{2}$$

2) Match-filter each of the N outputs from step 1 and retain the time of the maximum amplitude.

3) Find the largest subset of the N time points from step 2 whose least-square fit to a straight line has a 100 ms gradient (time difference between the tones) with less than *Dt* uncertainty. The uncertainty factor should be chosen not to be smaller than the biggest pulse-to-pulse time offset. With 1.6 s between the first and the last transmitted pulse, the biggest time offset will be $Dt = 1.6 \times v_s / c = 2.7$ ms to first approximation.

4) Set a confidence interval around the least square fit values from step 3 for every point. Check whether the points belong to the designated interval. Every point found outside the boundaries is deemed an outlier.

5) Repeat step 2 for each outlier in step 4, restricting the filtering to later or earlier times toward the least square estimate for that tone.

6) Repeat steps 3 to 5 until all the points are within the region of confidence specified by *Dt*.

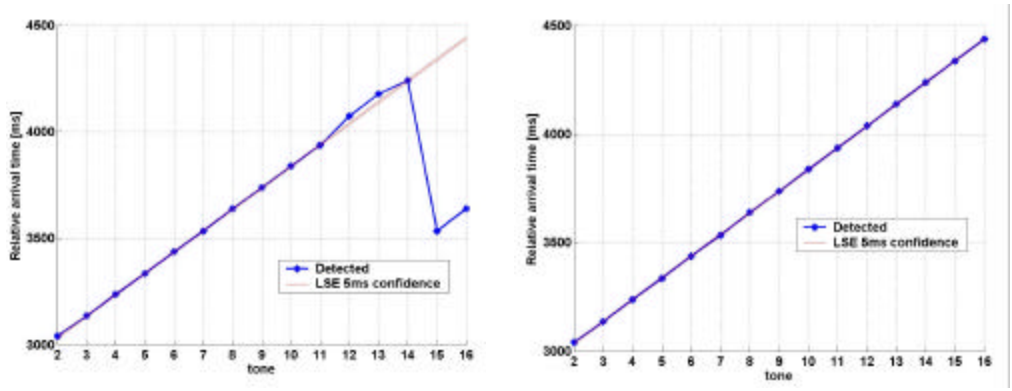

FIGURE 5. An example of a successful signal detection completed after two iterations. The line with symbols represents the times. The parallel straight lines delimit the 5ms confidence region of the least square fit.

Figure 5 shows an example of the iterations of this algorithm applied to the transmission sequence whose spectrogram is displayed in Fig. 2. After the initial iteration (Fig. 5a), 11 points of detected arrival times are in good agreement with the 100 ms tone-to-tone time difference. There is another group of two points about 100 ms apart, tones 15 (27 kHz) and 16 (30 kHz). They are the detected third harmonics of tones 7 (9 kHz) and 8 (10 kHz). Tones 12 and 13 are also on a line whose gradient is around 100ms. These two points probably belong to multipath arrivals. In step 3 of the algorithm, the largest group is chosen for the direct-path arrivals. At the second iteration, step 4 proceeds forward from the current estimated arrival times for tones 15 and 16, and backward for tones 12 and 13. A solution is reached when all the pulses are detected within a 5 ms tolerance interval (Fig. 5b). In these operations over the

limited data set, we did not use the 3 kHz signal, because its signal-to-noise ratio was often lower than the detection threshold. A repetitious false detection of one CW pulse would introduce high variance in the least square estimate, which would lead to slower convergence, and require redundant iterations. The potential direct-path arrival time at this frequency can be extrapolated from the measurements at the other frequencies. The output of the described example was used in plotting the circles in Fig. 2.

Coherent Summation of Correlograms

Since the data show that multipath arrivals were often much stronger than the direct-path arrivals, we developed an algorithm to search the correlograms for the global maximum, and for preceding local maxima that might correspond to the direct-path arrivals. Our rationale was that (1) detection results from one of the applied matched filters may help signal detection at other frequencies, for which the direct-path signal might have largely faded away, and/or the signal-to-noise ratio is below the detection threshold because of the bandwidth limitations of both the source transducer and the hydrophone (Fig. 1). Hence, by combining the correlograms for the 16 frequencies, one could take advantage of stronger signals at some frequencies to compensate for the limitations at others. And (2), the complexity of the algorithm should decrease by combining the correlograms into one generic sequence, and then searching one instead of N different sequences.

The algorithm starts with the broadband sequence y(m), which is digitized and recorded at the receiver, then band-pass filtered (impulse responses h_n) at each of the N transmitted frequencies:

$$x_n(m) = conv(y(m), h_n(m)), \;\; n = 1,..N \tag{3}$$

Next, outputs from the N filters are matched with a time-inverted replica h_M of the test signal, containing M samples, at the corresponding frequency [5]:

$$r_n(m) = conv(x_n(m), h_M^n(m)), \;\; n = 1,...N \tag{4}$$

$$\text{with} \;\; h_M^n(n) = x_n(M-1-m), \;\; m = 0,...M-1 \tag{5}$$

The resulting N correlograms (r_n) are then delayed *(N-n)T* time units, where *T* is the transmission time difference between two consecutive CW pulses (100 ms). To increase the accuracy, the time delay should be consistent with the ship's speed and the geometry of the problem. This operation aligns in time all the correlograms of one transmission sequence, before rectifying and summing them into a global correlogram r_s:

$$r_s(l) = \sum_{n=1}^{N} abs(r_n(l-(N-n)T \times f_s)), \;\; l = 1,...L \tag{6}$$

with sampling frequency f_s, and for a received sequence of length L. An example of such a global correlogram is shown in Fig. 6.

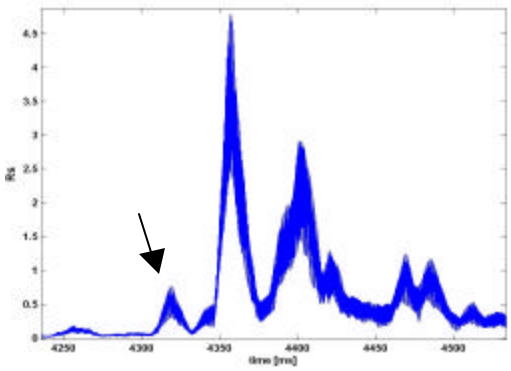

FIGURE 6. Sum of the 16 rectified correlograms received for one transmission sequence. The arrow points to the detected direct path arrival.

The algorithm searches the samples of the envelope of r_s, in the vicinity of the peak value, for a local maximum that might belong to the direct-path arrival.

Matches between segments of the sequence r_s, spanning ±10 ms around each detected local maximum, and an auto-correlation template are evaluated through a cost function (7). The template is generated by the same set of operations leading to r_s, but they are applied to the known transmitted signal, weighted by the source function (Fig. 1). The template is therefore the sum the rectified auto-correlation of each transmitted CW pulse. We expect more distortions in the multipath than the direct-path signals; hence the direct-path should retain more coherence with the signal auto-correlation in the correlograms. Since each transmitted CW pulse is 10ms long, the auto-correlograms ideally should be 20 ms long [5].

If $\boldsymbol{I}$ local maxima higher than the detection threshold are found, a cost function $c(i)$ is used to select one of them:

$$c(i) = \sum_{k=-K}^{K} \left| \frac{r_s^{template}(k) - r_s^{measured}(p(i)-k)}{r_s^{template}(k)} \right| \quad i = 0,\ldots I-1 \tag{7}$$

where K is the number of samples equivalent to the duration of each CW pulse (10 ms). A sample $\boldsymbol{p}$ will be selected as the end of the direct-path signal arrival, if it is the earliest of all the samples for which the cost function is below the threshold:

$$p_{dpa} = \min\left(p(i) \middle| c(i) < threshold \right) \tag{8}$$

For example, p_{dpa} was about 4320 ms in Fig. 6. If none of the local maxima satisfies the above criteria (7,8), the global maximum is retained as the direct-path arrival. The time of arrival for each CW pulse is then estimated by subtracting the corresponding time shift from (6):

$$p_n = p_{dpa} - (N-n)T \times f_s, \quad n = 1,\ldots N \tag{9}$$

TRANSMISSION LOSS ESTIMATION

The coherent sum of correlograms was used to estimate the propagation loss over one track at the Cortes-Tanner Banks site. The results are displayed in Figs. 7-8. Negative ranges correspond to the source moving towards the receiver. Detection threshold was set to 6 dB above the average noise power computed in each frequency band over a 100 ms time window, starting 2 s prior to each transmission sequence.

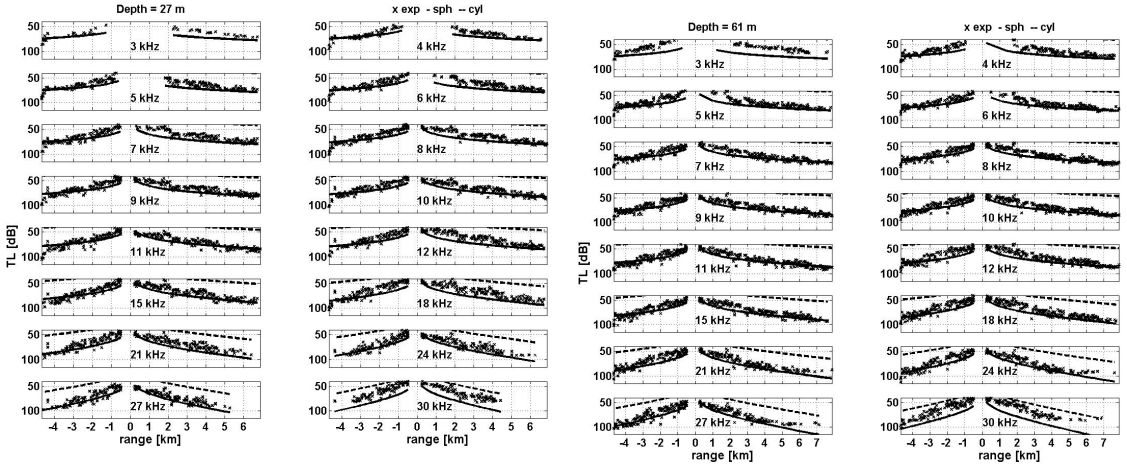

(a) **(b)**

FIGURE 7. Transmission loss vs. range at the 16 frequencies, measured at Cortes-Tanner Banks, for hydrophone depths of 27 m (a), and 61 m (b). The experimental results are marked with 'x', while solid and dashed line correspond to the theoretical transmission loss for absorption with spherical and cylindrical spreading, respectively.

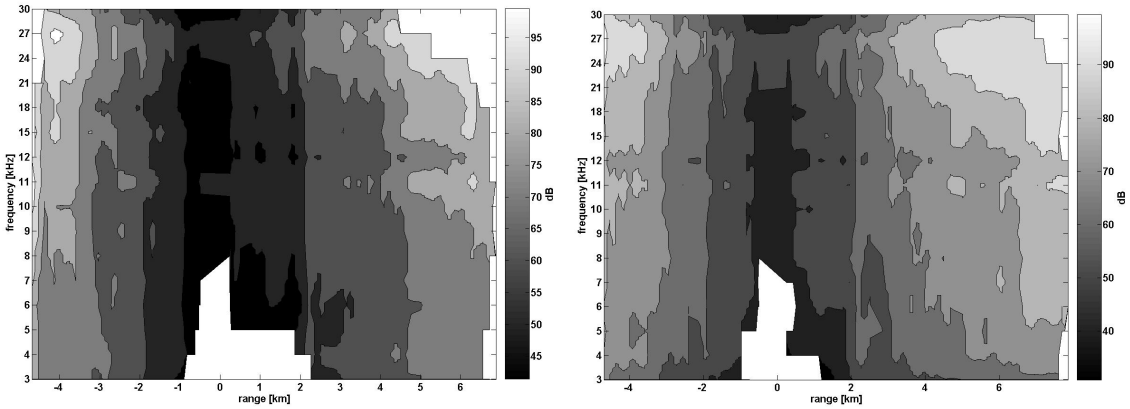

(a) **(b)**

FIGURE 8. Contours of transmission loss vs. range and frequency, measured at Cortes-Tanner Banks, for hydrophone depths of 27 m (a), and 61 m (b). The white regions correspond to SNR < 6 dB.

The experimental transmission loss values follow the theoretical spherical spreading and absorption [9-10] curves for all frequencies except for 3 kHz and 30 kHz (Fig. 7). Results shown in Fig. 8, excluding the regions with SNR lower than 6 dB, indicate that within the limited range (< 10 km) of the experiment, frequencies

below 6 kHz are more appropriate for signal transmission at either receiver depth (27 m and 61 m) for a source depth of about 40 m. It must be emphasized that these results correspond to direct-path attenuation in the 3-30 kHz band. In addition, low frequency (< 5 kHz) masking noise due to the towing vessel at short ranges, and low transmit response at 3 kHz and 30 kHz, as well as low receive sensitivity at 3 kHz (Fig. 1) were reasons for poor signal to noise ratio in the white range-frequency space in Fig. 8. Pending a more detailed range propagation study, we have assumed that no boundary interactions are involved, and that the frequency dependence is strictly due to absorption and scattering in the water column, as well as ambient noise. By contrast, results obtained at lower frequencies (e.g. 50 Hz - 3.2 kHz [11-13]) have shown that in waters shallower than 100 m, the optimum underwater acoustic communication frequency is around a few hundred Hz.

CONCLUSION

Direct-path transmission loss measurements were made with 16 CW pulses at frequencies from 3 kHz to 30 kHz. Two different methods of direct-path signal detection were implemented and tested on a limited data set. The first method detects each CW pulse independently and then applies a tone-to-tone time constraint to obtain a more accurate estimate of the direct-path arrival times of the pulses. The second algorithm is based on searching the recent history of the global maximum of the sum of the rectified correlograms received in a given transmission sequence.

The first method is robust against the inevitable timing offsets due to a moving transmitter, or nonlinear effects in the communication channel. The strength of the second method is its ability to merge the information from the CW pulses into a single function, and make a more reliable detection of the direct-path arrival for each tone in one step, whereas the first method requires a few iterations.

ACKNOWLEDGMENTS

For the experimental work that produced the data presented here, we wish to thank the Captain and crew of R/V New Horizon, Sean Wiggins who led the Feb. 2001 data collection, as well as Howard McManus, Seth Mogk, Carl Mattson, Scott Hiller, Earl Heckman, Erin Oleson and Melissa Hock who made all the pieces work together. P. Taylor and G. Wilkes of the US Naval Oceanographic Office funded the data collection work. A. Zoksimovski's MS thesis work is supported in part by the Center for Coastal and Ocean Mapping.

REFERENCES

1. http://www.itc-transducers.com
2. http://www.fas.org/man/dod-101/sys/ship/weaps/an-ssq-57.htm
3. U. S. Department of the Interior, POCS Technical Paper No. 82-2, *Physical Oceanography and Meteorology of the California Outer Continental Shelf*, August 1982.
4. Urick, R.J., *Principles of Underwater Sound*, McGraw-Hill, 1983.

5. Vaseghi, S.V., *Advanced Digital Signal Processing and Noise Reduction*, John Wiley, June 2000.
6. Ehrenberg, J.E., Ewart, T.E., and Morris, D.R., "Signal Processing techniques for resolving individual pulses in a multipath signal", *J. Acoust. Soc. Am.* **63(6)**, 1861-1865, (1978).
7. Moghaddam, P. P., Amindavar H., and Kirlin, R.L., "A new time-delay estimation in multipath", *IEEE Transactions on Signal Processing* **65**, 2503-2504 (1994).
8. Officer, C.B., *Introduction to the Theory of Sound Transmission – with application to the ocean*, McGraw-Hill, 1958.
9. François, R.E., and Garrison, G.R., "Sound absorption based on ocean measurements. I Pure water and magnesium sulfate contributions", *J. Acoust. Soc. Am.* **72(3)**, 896-907, (1982a).
10. François, R.E., and Garrison, G.R., "Sound absorption based on ocean measurements. II Boric acid contribution and equation for total absorption", *J. Acoust. Soc. Am.* **72(6)**, 1879-1890, (1982b).
11. Jensen, F.B., "Wave Theory Modeling: A Convenient Approach and Pulse Propagation Modeling in Low-Frequency Acoustics", *IEEE Journal of Oceanic Engineering*, vol. **13**, no. **4**, 186-197 (1988).
12. Jensen, F.B., and Kuperman, W.A., "Optimum frequency of propagation in shallow water environments", *J. Acoust. Soc. Am.* **73(3)**, 813-819 (1983).
13. Akal, T., *Effects of environmental variability on acoustic propagation loss in shallow water*, Impact of Littoral Environmental Variability on Acoustic Predictions and Sonar Performance – conference book, pp. 229-236, Kluwer Academic Publishers, 2002.